https://doi.org/10.5194/egusphere-2026-2429
Preprint. Discussion started: 8 May 2026

Brief Communication: Comparing ICESat-2 Altimetry and COSMO-SkyMed Synthetic Aperture Radar Interferometry Grounding Zone Products over Antarctica

Ankita Vashishtha[1], Pietro Milillo[1,2,3]

[1]Department of Civil and Environmental Engineering, University of Houston, Houston, TX, USA
[2]Department of Earth and Atmospheric Science, University of Houston, Houston, TX, USA
[3]German Aerospace Centre (DLR), Microwaves and Radar Institute, Munich, Germany

Correspondence to: Ankita Vashishtha (avashish@cougarnet.uh.edu)

Abstract

The grounding line represents a critical boundary in ice sheet dynamics, delineating the point at which an ice sheet detaches from its bed and begins to float as an ice shelf. Various methodologies have been developed to identify grounding lines, each leveraging distinct observational and processing techniques. However, there is a notable scarcity in the literature when it comes to comprehensive cross-comparisons of these different approaches. Here, we focus on a comparative analysis of a recent grounding line dataset derived from NASA's ICESat-2 altimetry data and the COSMO-SkyMed (CSK) synthetic aperture radar (SAR) imagery provided by the Italian Space Agency (ASI), covering Antarctica between 2020 and 2021. Across 73 Antarctic glaciers spanning ~69,440 km of grounding line, we evaluate the landward limit of tidal flexure (F), break in slope (I_b), and inland hydrostatic limit (H). Results indicate an average discrepancy relative to DInSAR grounding lines of 177 ±325 meters (F), 40 ± 830 meters (I_b), and 4508 ± 2731 meters (H). Contrary to the expectation that F lies closest to the grounding line, the F-GL discrepancy exceeds the I_b – GL discrepancy, reversing the expected ranking (F< I_b <H). Our findings advocate for the continued development and cross-validation of diverse methodologies to enhance the precision of ice sheet boundary monitoring and improve understanding of Antarctic ice dynamics.

1 Introduction

The grounding zone (GZ) marks the critical transition where ice, firmly anchored to bedrock, gives way to ice that floats freely as part of the ice shelves (Friedl et al., 2020). This boundary is essential for understanding ice sheet stability, as its position reflects the balance between ice-flow dynamics and ocean-driven melting. Changes in the GZ location can serve as an early indicator of ice sheet retreat or advance, directly influencing sea level projections. Accurate mapping of the grounding zone is fundamental for assessing ice mass loss and predicting potential contributions to global sea level rise. In the grounding zone several points can be identified in terms of the landward limit of tidal flexure (F), the true grounding line (G), the first point of

https://doi.org/10.5194/egusphere-2026-2429
Preprint. Discussion started: 8 May 2026

hydrostatic equilibrium (J), the break in slope (I_b), the local elevation minimum in GZ (I_m) and the inland limit of hydrostatic equilibrium (H) Figure 1 (Brunt et al., 2010; Ross et al 2024; Friedl et al., 2020; Li et al., 2022).

Grounding zone mapping techniques rely on various remote sensing methods (Friedl et al., 2020) including differential synthetic aperture radar interferometry (DInSAR), which is known for its high accuracy in detecting vertical ice displacements, repeat track laser altimetry (RTLA), used to identify elevation changes over time associated with tidal flexure and pseudo crossover radar altimetry (PCRA), which calculates surface elevation changes to detect ice-ocean interface. In addition, surface slope-based methods utilizing digital elevation models (DEMs) or optical imagery determine the break in slope, serve as proxies for grounding lines (Li et al. 2020; Li et al. 2022). Here, we compare the CSK DInSAR-mapped Grounding Line from Ross et al. (2025a) with the ICESat-2 RTLA-retrieved grounding zone product from Li et al. (2022).

Literature studies comparing these techniques are limited for several reasons, including the spatiotemporal availability of overlapping datasets and differences in the proxy measurements used to define grounding lines. Such limitations pose a challenge, as each technique may capture slightly different aspects of the ice-ocean interface. Additionally, specialized processing requirements hinder comprehensive cross-technique evaluations. The recent availability of ICESat-2 grounding zone products at NSIDC (Li et al. 2020) has provided an extended reference product that can be used for intercomparison. This dataset exploits ICESat-2's laser altimetry to map grounding zones, including flexure zone boundaries. The grounding line elevation-based data provides significant temporal and spatial coverage improvements. It facilitates more robust analyses by allowing scientists to cross-examine different techniques and refine grounding line assessments with enhanced accuracy and consistency. In their study (Li et al., 2022), they have analysed ICESat-2 repeat track data spanning from March 30, 2019, to September 30, 2020, validating it with Sentinel-1 DInSAR observations from 2018. These datasets, however, do not perfectly overlap in time and are restricted to the Filchner–Ronne and Ross ice shelves. Moreover, Sentinel-1 limitations in mapping GZ have been highlighted, particularly for fast glaciers in East and West Antarctica, such as Thwaites and Pine Island (Milillo et al., 2017; Milillo et al., 2019; Brancato et al., 2020; Milillo et al., 2022). In our study, we extend this validation approach and compare DInSAR data from the Italian COSMO-SkyMed constellation acquired at nearly the same period of 2020-2021 as the ICESat-2 observations and covering 73 glaciers and ice shelves in the Antarctic continent (Figure 1). Although the datasets are not strictly contemporaneous, this temporal offset is acceptable given the relatively slow evolution of grounding-line migration at continental scales and the multi-year configuration of DInSAR-derived products.

https://doi.org/10.5194/egusphere-2026-2429
Preprint. Discussion started: 8 May 2026

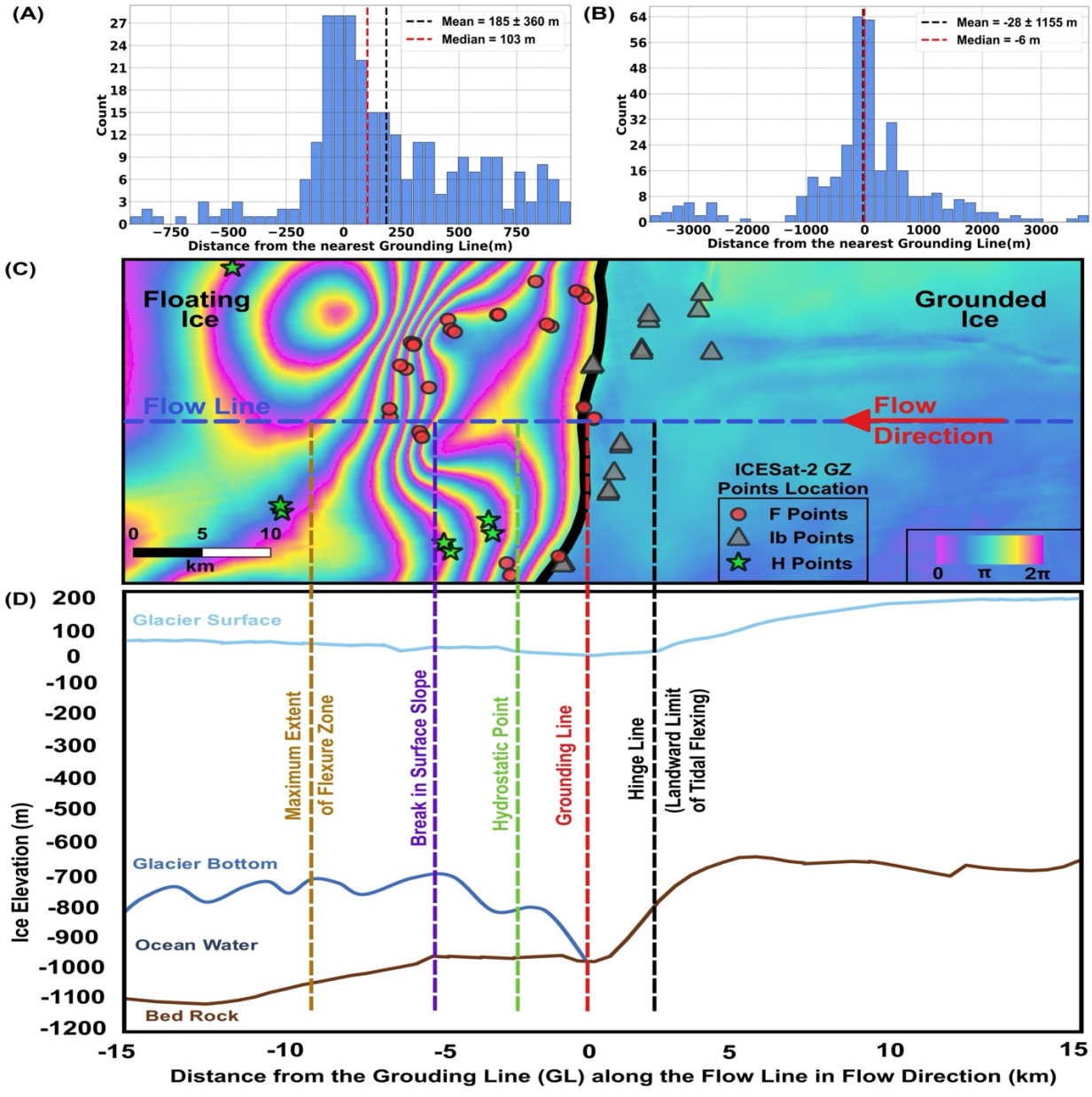

Figure 1 Bailey Ice Stream, East Antarctica, (A) Histogram of F point, (B) Histogram of I_b point distribution, (C) Visualization of glacier geometry observed in a DInSAR interferogram, red circle stands for F point location, gray triangle stands for Ib point location and green star stands for H point location for ICESat-2 data for grounding zone data, (D) Plot of Ice elevation and distance from the grounding line with ideal location of grounding zone points of a glacier. Glacier surface and bedrock profiles extracted from BedMachine Antarctica (Morlighem et al., 2017) along the profile line indicated in blue in (C). Glacier's bottom profile is unknown and was assumed for visualization purposes.

https://doi.org/10.5194/egusphere-2026-2429
Preprint. Discussion started: 8 May 2026

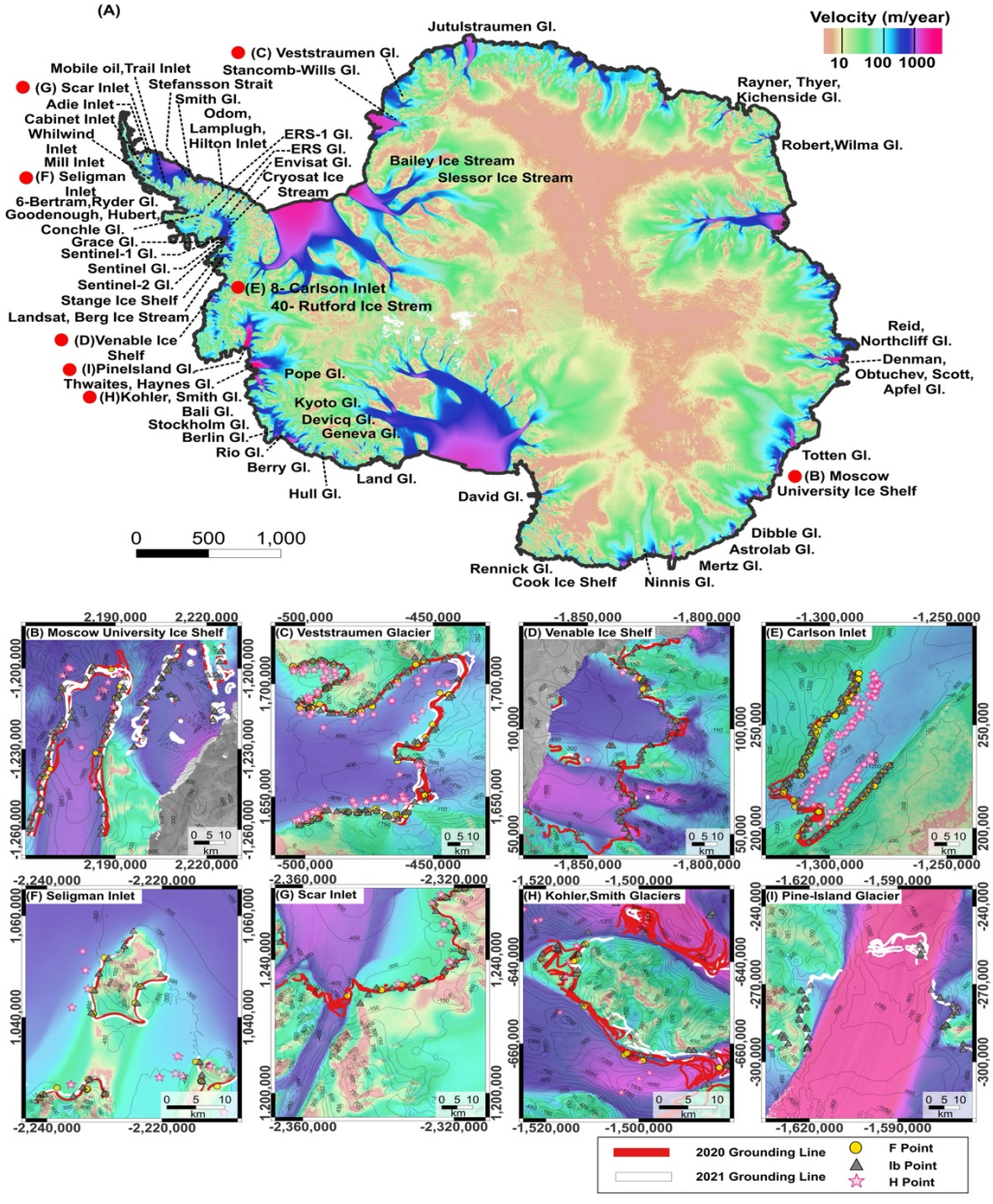

Figure 2 (A) Map of the Antarctica region showing the location of 73 glaciers (Table 1) in the EPSG 3031 map projection. Grounding lines and grounding zone product data are superimposed on the velocity magnitudes from 1996 to 2016 (Mouginot et al., 2017). Gl. stands for glacier in the figure. Red dots represent glaciers highlighted in panels B-I. Grounding lines at several glaciers (B) Moscow University glacier, (C) Veststraumen glacier, (D) Venable ice shelf, (E) Carlson inlet, (F) Seligman inlet, (G) Scar inlet, (H) Kohler, Smith glaciers, (I) Pine Island glacier. The yellow circle stands for F points, the gray triangle stands for Ib points, and the pink star stands for H points location for ICESat-2 grounding zone data.

https://doi.org/10.5194/egusphere-2026-2429
Preprint. Discussion started: 8 May 2026

2 Method

2.1 The CSK DInSAR dataset

The CSK DInSAR dataset from (Ross et al., 2025a) is generated from radar data acquired through the high-resolution SAR constellation managed by the Italian Space Agency (ASI). This dataset has been proven fundamental for accurately mapping the grounding lines of Antarctic and Greenland glaciers using the DInSAR technique (Milillo et al., 2017; Milillo et al., 2019; Brancato et al., 2020; Milillo et al., 2022; Millan et al., 2022; Ciracì et al., 2023; Ross et al., 2024). The DInSAR method exploits repeat-pass satellite acquisitions to detect vertical ice displacements induced by tides to identify the grounding line. The CSK system's capability for frequent, short-repeat acquisitions enables precise tracking of ice dynamics, even in fast-flowing regions. Such processing has been showcased in recent works (Ross et al. 2025a; Ross et al., 2025b; Ross et al., 2024 ; Milillo et al., 2019; Brancato et al., 2020; Milillo et al., 2022) and has provided so far invaluable insights for monitoring ice sheet stability and advancing climate-related research. Here, we analyse 73 glaciers and ice shelves in Antarctica (Ross et al., 2025a), as described in Figure 2 and Table S1.

2.2 ICESat-2 dataset

ICESat-2 grounding zone data is generated by processing the Land Ice Along-Track Height Product (ATL06) version 3 by utilizing repeat tracks from different cycles and by "re-tiding" the ocean loading tide (Li et al. 2020; Li et al., 2022). Poor-quality elevation measurements are removed by the ATL06_quality_summary flag. The along-track slope parameter is used to ensure height consistency between neighbouring elevation measurements by maintaining less than 2m distance between the original and the estimated elevations. Following the calculation of elevation anomalies, GZ points are identified. The GZ points F and H are identified based on the transition points from mean absolute elevation anomaly (MAEA) (Li et al., 2022). Point F is identified as the location where the gradient of the MAEA first increases from zero, and the second derivative of the MAEA reaches its positive peak. Point H is identified as the position where the gradient of the MAEA decreases to zero and the second derivative reaches its negative peak. I_b point is identified by calculating the low-pass-filtered reference elevation profile (Li et al., 2022). The location of the I_b point is considered the highest slope break between the two closest slope breaks.

2.3 Distance of ICESat-2 GZ points from CSK Grounding Lines

The GZ product data consists of points F, I_b, and H, which are compared with DInSAR grounding lines by calculating the closest distance of the points from the nearest grounding line on each glacier over the Antarctica region. Buffer distances of 1km, 5km, and 10 km are selected for F, I_b, and H points, respectively, to account for the spatially distributed nature of the grounding zone. These buffer values are consistent with the typical grounding zone width (Friedl et al., 2020) and are supported by observed separations between ICESat-2-derived ground zone points and DInSAR-mapped grounding lines (Li et al., 2022). A positive and negative sign convention is used to distinguish points located downstream and upstream of the reference line,

https://doi.org/10.5194/egusphere-2026-2429
Preprint. Discussion started: 8 May 2026

respectively. We have also calculated the percentage of total grounding line lengths for regions where ICESat-2 GZ products are not available.

Table 1: Cross comparison of F, I_b, and H ICESat-2 grounding zone product with DInSAR-mapped Grounding lines. Positive values stand for downstream and negative values stand for upstream location of the ICESat-2 dataset compared to DInSAR COSMO-SkyMed. In the table, Min stands for Minimum, Max stands for Maximum, and CV stands for Coefficient of Variation.

Points Name	No. of Points	Mean Distance + Standard deviation (m)	Min Distance (m)	Max Distance (m)	CV	Median (m)	Points in upstream	Points in Down stream	Percentage of total grounding line with no data points
East Antarctica: Total 25 glaciers and ice streams									
F	595	179±330	-926	995	1.8	112	176 (30%)	419 (70%)	72
I_b	1654	-108±972	-4856	3809	9	1	837 (51%)	817 (49%)	36
H	568	4495±2501	-4970	9974	0.6	4743	24 (4%)	544 (96%)	74
West Antarctica: Total 19 glaciers and ice streams									
F	375	227±331	-800	970	1.5	152	97 (26%)	278 (74%)	73
I_b	1515	206±674	-3362	4983	3.3	91	503 (33%)	1012 (67%)	27
H	301	5594±3124	-5363	9991	0.6	6356	11 (4%)	290 (96%)	79
Antarctica Peninsula: Total 29 glaciers and ice streams									
F	269	100±286	-851	971	2.9	56	95 (35%)	174 (65%)	78
I_b	805	12±732	-4849	4026	59	19	356 (44%)	449 (56%)	42
H	223	3035±1899	-9495	8233	0.6	2994	4 (2%)	219 (98%)	72
Antarctica: Total 73 glaciers and ice streams									
F	1239	177±325	-926	995	1.8	107	368 (30%)	871 (70%)	73
I_b	3974	40±830	-4856	4983	21	28	1696 (43%)	2278 (57%)	34
H	1092	4508±2731	-9495	9991	0.61	4523	39 (4%)	1053 (96%)	75

https://doi.org/10.5194/egusphere-2026-2429
Preprint. Discussion started: 8 May 2026

3 Results and Discussion

In Table 1, we have cross-compared about 6305 ICESat-2 derived points subdivided into 20%,63%, and 17% in F, I_b, and H points, respectively, across 73 glaciers. About 70% of the points representing the landward limit of tidal flexure (F points) are located downstream of the DInSAR grounding line at a mean distance of 177±325 m with a median distance of 107 m and maximum discrepancies of the order of 1 km either upstream or downstream the DInSAR-mapped grounding lines (Table 1). The F points matching accuracy with InSAR decreases over the glaciers located in West Antarctica, where we measure F 227±331 m downstream of the DInSAR-measured grounding lines. The value of CV varies from 1.5 to 2.9, indicating moderate variability, which suggests that ICESat-2 points consistently cluster within the tidal flexure zone near the DInSAR grounding line. In addition, 73% of DInSAR-mapped grounding lines are not mapped by corresponding F Points, including 15 entire glaciers (Astrolabe, Bertram, Ryder, ERS, Envisat, Grace, Hull, Landsat, Berg, Pine-Island, Reid, Northcliffe, Sentinel, Thwaites, Haynes) with no F points. The ICESat-2 mapped break in slope (I_b) points are mapped at a mean distance of 40±830 m downstream to the CSK DInSAR grounding lines(Table 1) with a median distance of 28 m. This is somewhat expected as I_b points are typically considered a less reliable representation of the true grounding line (G) compared to the landward limit of tidal flexure (Point F) (Dawson & Bamber, 2017; Freer et al., 2023; Fricker et al., 2009). For I_b points, we measure maximum discrepancies of the order of 5 km either upstream or downstream of the DInSAR-mapped grounding lines (Table 1). I_b points statistics change significantly depending on each Antarctic sector. In East Antarctica, over 1654 I_b points analysed, we record a mean distance of -108±972 and a median of 1m. Similarly, in the West Antarctica region, we found that about 67% of the I_b points are positioned downstream of the grounding line at a mean distance of 206±674 m, which is the highest among the East, West, and Peninsula regions. In the Peninsula region, among 805 I_b points, 56% are positioned downstream and 44% upstream at a mean distance of 12±732 m. I_b points in GZ product are available on all the glaciers in varying numbers, with only 34% of DInSAR-mapped GL not currently mapped by ICESat-2. Also, the large variation in the CV values (3.3 to 59) indicates that ICESat-2- derived points are widely distributed both upstream and downstream of the DInSAR grounding line, reflecting complex grounding zone dynamics across Antarctica and the presence of multiple potential flexure points. The particularly high CV (~59) observed in the Peninsula region further reflects its highly heterogeneous glacier regime, fragmented ice shelves, and the sensitivity of I_b to local topographic variability, due to a relatively lower number of I_b points. The Inland limit of hydrostatic equilibrium (H point) is known to be the farthest point among the ones we analysed. In our study, we have compared 1092 ICESat-2 H points with the CSK DInSAR grounding line (Table 1) and calculated that 96% of the points lie downstream at a mean distance of 4508±2731m and a median distance of 4523 m. The remarkably low value of CV (~0.6) indicates that ICESat-2 systematically detects the H points upstream of the DInSAR grounding line in thick outlet glaciers. For 75% of the DInSAR grounding line, corresponding H points are not available, which includes 22 glaciers (Astrolabe, Berry, Bertram, Ryder, ERS, Envisat, Grace, Landsat, Berg, Mertz, Pope, Reid, Northcliff, Rio, Robert, Wilma, Sentinel, Sentinel-1, Smith, Stancomb-Wills, Thwaites, Haynes). A similar trend is observed in all the regions.

https://doi.org/10.5194/egusphere-2026-2429
Preprint. Discussion started: 8 May 2026

4 Conclusion

In this work, we have detected a total of 1239 F points, 3973 I_b points, and 1092 H points lying in proximity of the CSK grounding lines. Across 73 glaciers, we find that DInSAR grounding lines serve as a primary reference for validation, while acknowledging their known uncertainties in regions of fast-flowing ice. The overall agreement is strong, with mean separations on the order of hundreds of meters for F and I_b points, but several kilometres for H points. As anticipated, the altimetry-derived hydrostatic equilibrium points (H) were the farthest from the DInSAR grounding line (reflecting their more seaward, floating position). However, contrary to theoretical expectations and prior studies, the altimetric break-in-slope points (I_b) were closer to the DInSAR grounding line than the flexure-based F points in nearly all regions. In fact, the mean F–GL discrepancy (177±325m) was larger than the I_b –GL discrepancy (40±830m) on an Antarctic-wide basis, a reversal of the expected ranking ($F < I_b < H$). This is explained in Figure 1, which shows the location of F, I_b for the Bailey ice stream. However, we note that the I_b –GL offsets exhibit the largest standard deviations among the three ICESat-2 point classes, indicating that while I_b points appear closer to the DInSAR grounding line on average, this result is not statistically robust and should be interpreted with caution. A plausible explanation for the noisier behaviour of I_b measurements in ICESat-2 altimetry relates to both geophysical and methodological factors inherent to slope-based detection. As highlighted by Li et al. (2020, 2022), the break-in-slope point is derived from the static elevation profile, which is highly sensitive to small-scale surface roughness, crevassing, rift fields, and local depressions inside the grounding zone (e.g., ice plains and surface minima; Figure 4 in Li et al., 2022). These features can cause rapid along-track fluctuations in slope and curvature, making the identification of the true morphological inflection point more ambiguous. Because I_b does not rely on ocean-tide–induced elevation changes but instead on the second derivative of the filtered elevation profile, it may track local topographic artefacts rather than the structural break associated with the grounding line. Moreover, the algorithm used to identify I_b requires low-pass filtering and piecewise polynomial fitting to suppress crevasse-scale noise, yet Li et al. (2022) emphasize that even after filtering, highly crevassed or rapidly flowing glaciers (e.g., Thwaites, Kohler, and Pope; Figure 12g–i in Li et al., 2022) can exhibit slope-break signatures that deviate several kilometres from the true grounding line. The sensitivity of I_b to the choice of filtering window, bin size for RMS-height estimation, and piecewise-fit thresholds can introduce additional methodological noise, particularly in regions where surface slope transitions are gradual rather than sharp. Earlier studies show that I_b points can shift more landward of the grounding line for ice plains such as Pine Island glacier, and multiple I_b points may exist based on the complexity of the grounding zone (Fricker & Padman, 2006; Fricker et al., 2009). Together, these effects help explain why I_b points show higher variance in their offsets relative to CSK DInSAR grounding lines, even though their mean separation may appear smaller than that of F points.

From a broader perspective, our validation underscores both the promise and the current limitations of satellite altimetry for grounding line monitoring. On one hand, ICESat-2's dense along-track sampling has enabled the first high-resolution Antarctic grounding zone product, yielding tens of thousands of F, H, and I_b locations across the ice sheet (Li et al., 2022). This demonstrates a step-change in coverage and frequency, with altimetry capturing many regions (including some fast glaciers difficult to survey) that were previously hard to monitor continuously. The close agreement reported by Li et al.

https://doi.org/10.5194/egusphere-2026-2429
Preprint. Discussion started: 8 May 2026

(2020; 2022) in certain regions, for example, Larsen C Ice Shelf where ICESat-2 F points agreed with InSAR to within ~0.02 km, and the Filchner-Ronne/Ross sector where mean differences were are also ~0.02 km, confirms that in ideal conditions (slow-moving ice, sufficient tidal range, and concurrent data), altimetry-derived grounding points might approach the precision of InSAR techniques. On the other hand, our extensive comparison using near-contemporaneous DInSAR across diverse glaciers reveals that altimetry alone does not universally achieve such precision, especially in dynamically complex areas. The discrepancies observed, particularly the unexpected closeness of I_b points to the DInSAR lines over F points, serve as a caution that even "high-resolution" altimetric products have inherent uncertainties. They highlight the importance of considering tidally driven grounding line oscillations and the spatial-temporal sampling differences between measurement techniques when interpreting grounding line positions. For critical applications such as ice-sheet mass balance or modelling, an error of a few hundred meters in grounding line position can be significant; therefore, our findings emphasize that reliance on a single technique may lead to misidentification or misplacement of the grounding line in certain settings. In this context, our analysis also suggests that despite its larger mean separation, the F point exhibits substantially lower variance than I_b and therefore may provide a more stable and less noisy boundary for both modelling and observational studies that require consistent grounding line positioning.

Overall, this study reinforces the need for integrated, multi-sensor approaches to accurately monitor Antarctica's grounding lines. DInSAR remains the gold standard for pinpointing the instantaneous grounding line, capturing fine-scale spatial detail of tidal flexure with accuracies on the order of tens of meters. ICESat-2 altimetry, meanwhile, provides broad spatial coverage and repeat measurements that can detect temporal changes (including longer-term migrations and ice plain dynamics) at a continent-wide scale. Each method has distinct strengths and limitations. For example, InSAR can degrade in areas or periods of poor radar phase coherence or require expensive continuous acquisitions, whereas laser altimetry depends on repeat orbits and can miss the grounding line in very fast or low-tide-amplitude regions. By combining these techniques, the scientific community can leverage their complementarities: using altimetry to fill spatial or temporal gaps in InSAR coverage and using InSAR to calibrate and validate altimetric proxies (as done here). The unexpected performance of the slope-break (I_b) proxy in our results suggests that additional cross-validation is warranted; future efforts could refine altimetric detection algorithms (e.g., adjusting tidal thresholds or incorporating auxiliary data) so that the flexure-based points better capture the true grounding line in challenging areas. In addition, continued validation against independent datasets (including new SAR missions and even emerging methods such as GNSS or ground imagery, where available) will be crucial to quantify the accuracy limits of each approach. In conclusion, our findings advocate for sustained development of multi-method strategies to ensure that Antarctic grounding line positions are determined with the highest possible fidelity. This integrated approach will improve the robustness of ice sheet change assessments and enhance confidence in projections of sea-level rise stemming from grounding line retreat.

Acknowledgements

https://doi.org/10.5194/egusphere-2026-2429
Preprint. Discussion started: 8 May 2026

Author contributions: Both authors contributed to writing the paper. Analysis and visualization were conducted by A.V. Result interpretation and manuscript writing were carried out by A.V and P.M.

Funding

This work was conducted at the University of Houston, TX, under a contract with the Cryosphere Program of NASA and the NASA Decadal Survey Incubation program.

References

Brancato, V., Rignot, E., Milillo, P., Morlighem, M., Mouginot, J., An, L., Scheuchl, B., Jeong, S., Rizzoli, P., Bueso Bello, J. L., & Prats-Iraola, P.: Grounding Line Retreat of Denman Glacier, East Antarctica, Measured With COSMO-SkyMed Radar Interferometry Data, Geophysical Research Letters, 47(7), https://doi.org/10.1029/2019GL086291,2020.

Brunt, K. M., Fricker, H. A., Padman, L., Scambos, T. A., & O'Neel, S.: Mapping the grounding zone of the Ross Ice Shelf, Antarctica, using ICESat laser altimetry, Annals of Glaciology, 51(55), 71–79, https://doi.org/10.3189/172756410791392790, 2010.

Ciracì, E., Rignot, E., Scheuchl, B. I., Tolpekin, V. I., Wollersheim, M., An, L., Milillo, P., Bueso-Bello, J.-L. I., Rizzoli, P. I., Dini, L., Byron Parizek, R., & Robel, A. A.: Melt rates in the kilometer-size grounding zone of Petermann Glacier, Greenland, before and during a retreat, PNAS, 120(20), https://doi.org/10.1073/pnas, 2023.

Dawson, G. J., & Bamber, J. L.: Antarctic Grounding Line Mapping from CryoSat-2 Radar Altimetry, Geophysical Research Letters, 44(23), 11,886-11,893, https://doi.org/10.1002/2017GL075589, 2017.

Freer, B. I. D., Marsh, O. J., Hogg, A. E., Fricker, H. A., & Padman, L.: Modes of Antarctic tidal grounding line migration revealed by Ice, Cloud, and land Elevation Satellite-2 (ICESat-2) laser altimetry, The Cryosphere, 17(9), 4079–4101, https://doi.org/10.5194/tc-17-4079-2023, 2023.

Fricker, H. A., Coleman, R., Padman, L., Scambos, T. A., Bohlander, J., & Brunt, K. M.: Mapping the grounding zone of the Amery Ice Shelf, East Antarctica using InSAR, MODIS and ICESat. Antarctic Science, 21(5), 515–532, https://doi.org/10.1017/S095410200999023X, 2009.

Fricker, H. A., & Padman, L.: Ice shelf grounding zone structure from ICESat laser altimetry. Geophysical Research Letters, 33(15), https://doi.org/10.1029/2006GL026907, 2006

https://doi.org/10.5194/egusphere-2026-2429
Preprint. Discussion started: 8 May 2026

Friedl, P., Weiser, F., Fluhrer, A., & Braun, M. H.: Remote sensing of glacier and ice sheet grounding lines: A review, Earth-Science Reviews, Vol. 201, Elsevier B.V, https://doi.org/10.1016/j.earscirev.2019.102948, 2020.

Li, T., Dawson, G. J., Chuter, S. J., & Bamber, J. L.:Mapping the grounding zone of Larsen C Ice Shelf, Antarctica, from ICESat-2 laser altimetry, The Cryosphere, 14(11), 3629–3643, https://doi.org/10.5194/tc-14-3629-2020, 2020.

Li, T., Dawson, G. J., Chuter, S. J., & Bamber, J. L.: A high-resolution Antarctic grounding zone product from ICESat-2 laser altimetry, Earth System Science Data, 14(2), 535–557, https://doi.org/10.5194/essd-14-535-2022, 2022.

Milillo, P., Rignot, E., Mouginot, J., Scheuchl, B., Morlighem, M., Li, X., & Salzer, J. T.: On the Short-term Grounding Zone Dynamics of Pine Island Glacier, West Antarctica, Observed With COSMO-SkyMed Interferometric Data. Geophysical Research Letters, 44(20), 10,436-10,444, https://doi.org/10.1002/2017GL074320, 2017.

Milillo, P., Rignot, E., Rizzoli, P., Scheuchl, B., Mouginot, J., Bueso-Bello, J., & Prats-Iraola, P.: Heterogeneous retreat and ice melt of Thwaites Glacier, West Antarctica, Science Advances, Vol 5, Issue 1, https://www.science.org, 2019.

Milillo, P., Rignot, E., Rizzoli, P., Scheuchl, B., Mouginot, J., Bueso-Bello, J. L., Prats-Iraola, P., & Dini, L.: Rapid glacier retreat rates observed in West Antarctica, Nature Geoscience, 15(1), 48–53, https://doi.org/10.1038/s41561-021-00877-z, 2022.

Millan, R., Mouginot, J., Rabatel, A., & Morlighem, M.: Ice velocity and thickness of the world's glaciers, Nature Geoscience, 15(2), 124–129, https://doi.org/10.1038/s41561-021-00885-z, 2022.

Morlighem, M., Williams, C. N., Rignot, E., An, L., Arndt, J. E., Bamber, J. L., Catania, G., Chauché, N., Dowdeswell, J. A., Dorschel, B., Fenty, I., Hogan, K., Howat, I., Hubbard, A., Jakobsson, M., Jordan, T. M., Kjeldsen, K. K., Millan, R., Mayer, L., … Zinglersen, K. B.:BedMachine v3: Complete Bed Topography and Ocean Bathymetry Mapping of Greenland From Multibeam Echo Sounding Combined With Mass Conservation, Geophysical Research Letters, 44(21), 11,051-11,061, https://doi.org/10.1002/2017GL074954, 2017.

Mouginot, J., Rignot, E., Scheuchl, B., & Millan, R.: Comprehensive annual ice sheet velocity mapping using Landsat-8, Sentinel-1, and RADARSAT-2 data, Remote Sensing, 9(4), https://doi.org/10.3390/rs9040364, 2017.

https://doi.org/10.5194/egusphere-2026-2429
Preprint. Discussion started: 8 May 2026

Ross, N., Milillo, P., & Dini, L.: Automated grounding line delineation using deep learning and phase gradient-based approaches on COSMO-SkyMed DInSAR data, Remote Sensing of Environment, 315, https://doi.org/10.1016/j.rse.2024.114429, 2024.

Ross, N., Milillo, P., & Dini, L.: Antarctic grounding line delineation from the Italian Space Agency COSMO-SkyMed DInSAR data, Scientific Data, 12(1), 1737, https://doi.org/10.1038/s41597-025-06023-3, 2025a.

Ross, N., Milillo, P., Nakshatrala, K., Ballarini, R., Stubblefield, A., & Dini, L.: Importance of ice elasticity in simulating tide-induced grounding line variations along prograde bed slopes, The Cryosphere, 19(6), 1995–2015, https://doi.org/10.5194/tc-19-1995-2025, 2025b.